

Nonlinear Predictive Control of Spacecraft

John L. Crassidis¹

F. Landis Markley²

Tobin C. Anthony³

Stephen F. Andrews³

Abstract

A new approach for the control of a spacecraft with large angle maneuvers is presented. This new approach is based on a nonlinear predictive control scheme which determines the required torque input so that the predicted responses match the desired trajectories. This is accomplished by minimizing the norm-squared local errors between the predicted and desired quantities. Formulations are presented which use either attitude and rate tracking or attitude-tracking alone. The robustness of the new controller with respect to large system uncertainties is also demonstrated. Finally, simulation results are shown which use the new control strategy to stabilize the motion of the Microwave Anisotropy Probe spacecraft.

Introduction

The control of spacecraft for large angle slewing maneuvers poses a difficult problem. Some of these difficulties include: the highly nonlinear characteristics of the governing equations, control rate and saturation constraints and limits, and incomplete state knowledge due to sensor failure or omission. The control of spacecraft with large angle slews can be accomplished by either open-loop or closed-loop schemes. Open-loop schemes usually require a pre-determined pointing maneuver and are typically determined using optimal control techniques, which involve the solution of a two-point boundary value problem (e.g., the time optimal maneuver problem¹). Also, open-loop schemes are sensitive to spacecraft parameter uncertainties and unexpected

¹ Assistant Professor, Dept. of Mech. Eng., The Catholic University of America, Washington, D.C. 20064. Senior Member AIAA.

² Staff Engineer, Goddard Space Flight Center, Code 712, Greenbelt, MD 20771. Associate Fellow AIAA.

³ Engineer, Goddard Space Flight Center, Code 712, Greenbelt, MD 20771.

disturbances.² Closed-loop systems can account for parameter uncertainties and disturbances, and thus provide a more robust design methodology.

In recent years, much effort has been devoted to the closed-loop design of spacecraft with large angle slews. Wie and Barba³ derive a number of simple control schemes using quaternion and angular velocity (rate) feedback. Asymptotic stability is shown by using a Lyapunov function analysis for all cases. Tsiotras⁴ expands upon these formulations by deriving simple control laws based on both a Gibbs vector parameterization and a modified Rodrigues parameterization, each with rate feedback (for a complete survey of attitude parameterizations see Ref. [5]). Lyapunov functions are shown for all the controllers developed in Ref. [4] as well. Other full state feedback techniques have been developed that are based on sliding mode (variable structure) control, which uses a feedback linearizing technique and an additional term aimed at dealing with model uncertainty.⁶ This type of control has been successfully applied for large angle maneuvers using a Gibbs vector parameterization,⁷ a quaternion parameterization,⁸ and a modified Rodrigues parameterization.⁹ Another robust control scheme using a nonlinear H_∞ control methodology has been developed by Kang.¹⁰ This scheme involves the solution of Hamilton-Jacobi-Isaacs inequalities, which essentially determines feedback gains for the full state feedback control problem so that the spacecraft is stabilized in the presence of uncertainties and disturbances. Another class of controllers involves adaptive techniques, which update the model during operation based on measured performances (e.g., see Ref. [6]). An adaptive scheme which estimates external torques by tracking a Lyapunov function has been developed by Schaub et. al.¹¹ This method has been shown to be very robust in the presence of spacecraft modeling errors and disturbances.

The aforementioned techniques all utilize full state knowledge (i.e., attitude and rate feedback). The problem of controlling a spacecraft without full state feedback is more complex. The basic approaches used to solve this problem can be divided into methods which estimate the unmeasured states using a filter algorithm, or methods which develop control laws directly from output feedback. Filtering methods, such as the extended Kalman filter, have been successfully applied on numerous spacecraft systems without the use of rate-integrating gyro measurements (e.g., see Refs. [12]-[14]). An advantage of these methods is that the attitude may be estimated by using only one set of vector attitude observations (such as magnetometer observations).

However, these methods are usually much less accurate than methods which use gyro measurements. A more direct technique has been developed by Lizarralde and Wen,¹⁵ which solves the attitude problem without rate knowledge. This method is based on a passivity approach, which replaces the rate feedback by a nonlinear filter of the quaternion. A model-based filter reconstructing the angular velocity is not needed in this case.

In this paper, a new method for the control of large angle spacecraft maneuvers is presented. This method is based on a nonlinear predictive controller for continuous systems with discrete observations, developed by Lu.¹⁶ The control law is based on the minimization of the norm-squared local errors between the controlled variables and desired values. Also, an input-constrained tracking problem¹⁷ is used for more realistic spacecraft applications. The nonlinear predictive controller has been successfully applied on numerous systems, such as nonlinear control of aircraft.¹⁸ Advantages of the new control scheme include: (i) the control law predicts the torque input by tracking a one-time step ahead trajectory, (ii) the controller is very robust with respect to spacecraft model uncertainties and disturbances, and (iii) the control scheme produces unbiased control errors.

The organization of this paper proceeds as follows. First, a brief summary of the kinematics and dynamics of a spacecraft is presented. Then, a brief overview of the nonlinear predictive control theory with input constraints is shown. Next, a nonlinear predictive control scheme is developed for the purpose of stabilizing a spacecraft with large angle maneuvers. Also, a robustness study is shown for scalar multiplicative uncertainties in the inertia matrix. Finally, simulation results are shown for the Microwave Anisotropy Probe (MAP) spacecraft.

Spacecraft Dynamics

In this section, a brief review of the kinematic and dynamic equations of motion for a three-axis stabilized spacecraft is shown. The attitude is assumed to be represented by the quaternion, defined as

$$\underline{q} \equiv \begin{bmatrix} q_{13} \\ q_4 \end{bmatrix} \quad (1)$$

with

$$\underline{q}_{13} \equiv \begin{bmatrix} q_1 \\ q_2 \\ q_3 \end{bmatrix} = \hat{n} \sin(\theta/2) \quad (2a)$$

$$q_4 = \cos(\theta/2) \quad (2b)$$

where \hat{n} is a unit vector corresponding to the axis of rotation and θ is the angle of rotation. The quaternion kinematic equations of motion are derived by using the spacecraft's angular velocity ($\underline{\omega}$), given by

$$\dot{\underline{q}} = \frac{1}{2} \Omega(\underline{\omega}) \underline{q} = \frac{1}{2} \Xi(\underline{q}) \underline{\omega} \quad (3)$$

where $\Omega(\underline{\omega})$ and $\Xi(\underline{q})$ are defined as

$$\Omega(\underline{\omega}) \equiv \begin{bmatrix} -[\underline{\omega} \times] & \vdots & \underline{\omega} \\ \cdots & \vdots & \cdots \\ -\underline{\omega}^T & \vdots & 0 \end{bmatrix} \quad (4a)$$

$$\Xi(\underline{q}) \equiv \begin{bmatrix} q_4 I_{3 \times 3} + [\underline{q}_{13} \times] \\ \cdots \\ -\underline{q}_{13}^T \end{bmatrix} \quad (4b)$$

where $I_{n \times n}$ represents a $n \times n$ identity matrix (also, $0_{n \times m}$ will represent a $n \times m$ zero matrix). The 3×3 dimensional matrices $[\underline{\omega} \times]$ and $[\underline{q}_{13} \times]$ are referred to as cross product matrices since $\underline{a} \times \underline{b} = [\underline{a} \times] \underline{b}$, with

$$[\underline{a} \times] \equiv \begin{bmatrix} 0 & -a_3 & a_2 \\ a_3 & 0 & -a_1 \\ -a_2 & a_1 & 0 \end{bmatrix} \quad (5)$$

Since a three degree-of-freedom attitude system is represented by a four-dimensional vector, the quaternion components cannot be independent. This condition leads to the following normalization constraint

$$\underline{q}^T \underline{q} = \underline{q}_{13}^T \underline{q}_{13} + q_4^2 = 1 \quad (6)$$

Also, the matrix $\Xi(\underline{q})$ obeys the following helpful relations

$$\Xi^T(\underline{q}) \Xi(\underline{q}) = \underline{q}^T \underline{q} I_{3 \times 3} \quad (7a)$$

$$\Xi(\underline{q}) \Xi^T(\underline{q}) = \underline{q}^T \underline{q} I_{4 \times 4} - \underline{q} \underline{q}^T \quad (7b)$$

$$\Xi^T(\underline{q}) \underline{q} = \underline{0}_{3 \times 1} \quad (7c)$$

$$\Xi^T(\underline{q}) \underline{\lambda} = -\Xi^T(\underline{\lambda}) \underline{q} \text{ for any } \underline{\lambda}_{4 \times 1} \quad (7d)$$

Also, the error quaternion of two quaternions, \underline{q} and $\tilde{\underline{q}}$, is defined by

$$\underline{\delta q} \equiv \begin{bmatrix} \frac{\delta q_{13}}{\dots} \\ \dots \\ \dots \\ \delta q_4 \end{bmatrix} = \underline{q} \otimes \tilde{\underline{q}}^{-1} \quad (8)$$

where the operator \otimes denotes quaternion multiplication (see Ref. [3] for details), and the inverse quaternion is defined by

$$\tilde{\underline{q}}^{-1} = [-\tilde{q}_1 \quad -\tilde{q}_2 \quad -\tilde{q}_3 \quad \tilde{q}_4]^T \quad (9)$$

Another useful identity is given by

$$\underline{\delta q}_{13} = \Xi^T(\tilde{\underline{q}}^{-1}) \underline{q} \quad (10)$$

Also, if Equation (8) represents a small rotation then $\delta q_4 \approx 1$, and $\underline{\delta q}_{13}$ corresponds to half-angles of rotation.

The dynamic equations of motion, also known as Euler's equations, for a rotating spacecraft are given by¹⁹

$$\dot{\underline{H}} = -\underline{\omega} \times \underline{H} + \underline{u}_{\text{ext}} \quad (11)$$

where \underline{H} is the total system angular momentum, $\underline{u}_{\text{ext}}$ is the total external torque (which includes, control torques, aerodynamic drag torques, solar pressure torques, etc.). Also, the angular velocity form of Euler's equation can be used, given by

$$J \dot{\underline{\omega}} = -\underline{\omega} \times (J \underline{\omega}) + \underline{u} \quad (12)$$

where J is the inertia matrix of the spacecraft, and \underline{u} is the total torque. Equations (8), (9), and (12) can be used to show that rotational motion without nutation occurs only if the rotation is about a principal axis of the rigid body (see Ref. [19] for details).

Nonlinear Predictive Control

Preliminaries

In this section, the nonlinear predictive control algorithm is summarized (see Ref. [16] for more details). In the nonlinear predictive controller it is assumed that the system is modeled by

$$\dot{\underline{x}}(t) = \underline{f}(\underline{x}(t)) + G(\underline{x}(t))\underline{u}(t) \quad (13a)$$

$$\underline{y}(t) = \underline{c}(\underline{x}(t)) \quad (13b)$$

where $\underline{f}: \mathbb{R}^n \rightarrow \mathbb{R}^n$ is sufficiently differentiable, $\underline{x}(t) \in \mathbb{R}^n$ is the state vector, $\underline{u}(t) \in \mathbb{R}^q$ represents the control-input vector, $G(\underline{x}(t)) : \mathbb{R}^n \rightarrow \mathbb{R}^{n \times q}$ is the control-input distribution matrix, $\underline{c}(\underline{x}(t)) : \mathbb{R}^n \rightarrow \mathbb{R}^m$ is the observation vector, and $\underline{y}(t) \in \mathbb{R}^m$ is the output vector.

A Taylor series expansion of the output estimate in Equation (13b) is given by

$$\underline{y}(t + \Delta t) \approx \underline{y}(t) + \underline{z}(\underline{x}(t), \Delta t) + \Lambda(\Delta t) S(\underline{x}(t)) \underline{u}(t) \quad (14)$$

where the i^{th} element of $\underline{z}(\underline{x}(t), \Delta t)$ is given by

$$z_i(\underline{x}(t), \Delta t) = \sum_{k=1}^{p_i} \frac{\Delta t^k}{k!} L_f^k(c_i) \quad (15)$$

where p_i , $i = 1, 2, \dots, m$, is the lowest order of the derivative of $c_i(\underline{x}(t))$ in which any component of $\underline{u}(t)$ first appears due to successive differentiation and substitution for $\dot{x}_i(t)$ on the right side.

$L_f^k(c_i)$ is a k^{th} order Lie derivative, defined by

$$\begin{aligned} L_f^k(c_i) &= c_i && \text{for } k = 0 \\ L_f^k(c_i) &= \frac{\partial L_f^{k-1}(c_i)}{\partial \underline{x}} f && \text{for } k \geq 1 \end{aligned} \quad (16)$$

$\Lambda(\Delta t) \in \mathbb{R}^{m \times m}$ is a diagonal matrix with elements given by

$$\lambda_{ii} = \frac{\Delta t^{p_i}}{p_i!}, \quad i = 1, 2, \dots, m \quad (17)$$

$S(\underline{x}(t)) \in \mathbb{R}^{m \times q}$ is a matrix with each i^{th} row given by

$$s_i = \left\{ L_{g_1} \left[L_f^{p_i-1}(c_i) \right], \dots, L_{g_q} \left[L_f^{p_i-1}(c_i) \right] \right\}, \quad i = 1, 2, \dots, m \quad (18)$$

where the Lie derivative with respect to L_{g_j} in Equation (18) is defined by

$$L_{g_j} \left[L_f^{p_i-1}(c_i) \right] \equiv \frac{\partial L_f^{p_i-1}(c_i)}{\partial \underline{x}} g_j, \quad j = 1, 2, \dots, q \quad (19)$$

Equation (19) is in essence a generalized sensitivity matrix for nonlinear systems.

Nonlinear Control

A cost functional consisting of the weighted sum square of the desired-minus-actual residuals plus the weighted sum square of the model correction term is minimized, given by

$$J(\underline{u}(t)) = \frac{1}{2} \underline{e}(t + \Delta t)^T R \underline{e}(t + \Delta t) + \frac{1}{2} \underline{u}^T(t) W \underline{u}(t) \quad (20)$$

where $\underline{e}(t + \Delta t) = \underline{\tilde{y}}(t + \Delta t) - \underline{y}(t + \Delta t)$. The weighting matrices $W \in \mathbb{R}^{q \times q}$ and $R \in \mathbb{R}^{m \times m}$ are control-input and output-tracking weighting matrices, respectively. Also, $\underline{\tilde{y}}(t + \Delta t)$ represents

the desired output. Substituting Equation (14), and minimizing Equation (20) with respect to $\underline{u}(t)$ leads to the following control input

$$\underline{u}(t) = -\left\{\left[\Lambda(\Delta t)S(\underline{x})\right]^T R \Lambda(\Delta t) S(\underline{x}) + W\right\}^{-1} \left[\Lambda(\Delta t)S(\underline{x})\right]^T R \left[\underline{z}(\underline{x}, \Delta t) - \underline{\tilde{y}}(t + \Delta t) + \underline{y}(t)\right] \quad (21)$$

Equation (21) is used to perform a one-time step ahead control of the nonlinear system to the desired value at time $t + \Delta t$.

The constrained-input case is defined by placing bounds on the control input, given by

$$L_i(\underline{x}, t) \leq u_i(t) \leq U_i(\underline{x}, t), \quad i = 1, 2, \dots, q \quad (22)$$

where $L_i(\underline{x}, t)$ and $U_i(\underline{x}, t)$ are given continuous functions of their arguments. Next, the saturation function is defined by

$$\text{sat}_i(\underline{u}) = \begin{cases} U_i, & u_i \geq U_i \\ u_i, & L_i < u_i < U_i \\ L_i, & u_i \leq L_i \end{cases} \quad (23)$$

The unique optimal control is the solution of the following fixed-point equation (see Ref. [17] for details)

$$\underline{u} = \rho(\underline{u}) = \text{sat}\left\{\mu S^T \Lambda R \left(\underline{e}^\Delta - \underline{z}\right) - \left[\mu \left(S^T \Lambda R \Lambda S + W\right) - I\right] \underline{u}\right\} \quad (24)$$

where $\underline{e}^\Delta \equiv \underline{\tilde{y}}(t + \Delta t) - \underline{y}(t)$, and all other arguments have been suppressed for clarity. The variable μ is defined by

$$\mu = \left\{ \sum_{i=1}^q \sum_{j=1}^q \left[S^T \Lambda R \Lambda S + W \right]_{ij}^2 \right\}^{-1/2} \quad (25)$$

The fixed point iteration sequence is generated by $\underline{u}^k = \rho(\underline{u}^{k-1})$, which typically converges in a few iterations. Note that Equation (24) is not the same as Equation (21) with a saturation mapping applied to the right hand side, unless $S^T \Lambda R \Lambda S + W$ happens to be diagonal.

Spacecraft Predictive Control

In this section a nonlinear predictive controller is developed for spacecraft applications. The output equation is assumed to be equivalent to the state equation, so that

$$\underline{y} = \underline{x} = \begin{bmatrix} \underline{q} \\ \underline{\omega} \end{bmatrix} \quad (26)$$

with state equations given by Equations (3) and (12). The lowest order derivative of $\underline{\omega}$ where \underline{u} first appears is 1, and the lowest order derivative of \underline{q} where \underline{u} first appears is 2. Therefore, Equation (17) becomes (suppressing arguments for simplicity)

$$\Lambda = \frac{1}{2} \begin{bmatrix} \Delta t^2 I_{4 \times 4} & 0_{4 \times 3} \\ 0_{3 \times 4} & 2 \Delta t I_{3 \times 3} \end{bmatrix} \quad (27)$$

Using Equation (18) the $S(\underline{x})$ matrix can be shown to be

$$S(\underline{x}) = \begin{bmatrix} \frac{1}{2} \Xi(\underline{q}) J^{-1} \\ J^{-1} \end{bmatrix} \quad (28)$$

It can also be shown that the matrix inverse in Equation (21) is constant by using the identity in Equation (7a) and if R is given by

$$R = \begin{bmatrix} r_q I_{4 \times 4} & 0_{4 \times 3} \\ 0_{3 \times 4} & r_\omega I_{3 \times 3} \end{bmatrix} \quad (29)$$

where r_q and r_ω are scalars. This fact makes the control law particularly well suited for computer implementation. Also, it is important to note that the control law in Equation (21) is driven by both a quaternion and angular velocity *difference*. Differencing or adding quaternions in any application is not usually desired, since the resulting quaternion may not have unit norm. However, the correction for the quaternion is in actuality a *multiplicative* correction. This is due to the structure of Equation (28) and from the identities in Equations (7d) and (10). For a more complete discussion on additive and multiplicative quaternion corrections see Ref. [20]. The vector \underline{z} formed by using Equation (15) can be shown to be given by

$$\underline{z} = \begin{bmatrix} \underline{z}_q \\ \dots \\ \underline{z}_\omega \end{bmatrix} \quad (30)$$

where

$$\underline{z}_q = -\frac{\Delta t^2}{8} \{ (\underline{\omega} \cdot \underline{\omega}) \underline{q} + 2 \underline{\Xi}(\underline{q}) J^{-1} [\underline{\omega} \times] J \underline{\omega} \} + \frac{\Delta t}{2} \underline{\Xi}(\underline{q}) \underline{\omega} \quad (31a)$$

$$\underline{z}_\omega = -\Delta t J^{-1} [\underline{\omega} \times] J \underline{\omega} \quad (31b)$$

Note that the $(\underline{\omega} \cdot \underline{\omega}) \underline{q}$ in Equation (31a) vanishes when used in Equation (21), due to the identity in Equation (7c), if Equation (29) holds true.

Robustness

In this section, a robustness study is shown for scalar perturbations in the assumed inertia matrix (i.e., assuming that the modeled inertia matrix perturbation is given by $\alpha(t) J$, where $\alpha(t)$ is a scalar, continuous function with bound given by $0 < \alpha(t) < \delta$). For simplicity the regulation case is considered only, so that \underline{q} is the identity quaternion and $\underline{\omega} = \underline{0}$ for $t \in [0, t_f]$.

Also, it is assumed that the control weighting matrix (W) is zero. Under these conditions and perturbation, Euler's equation in Equation (12) can be shown to be given by

$$\dot{\underline{\omega}} = (\alpha - 1) J^{-1} [\underline{\omega} \times] J \underline{\omega} - \alpha \gamma \underline{\omega} - \alpha \beta \underline{q}_{13} \quad (32)$$

where

$$\beta = \frac{4 r_q}{(\Delta t^2 r_q + 16 r_\omega)} \quad (33a)$$

$$\gamma = \frac{2(\Delta t^2 r_q + 8 r_\omega)}{\Delta t(\Delta t^2 r_q + 16 r_\omega)} \quad (33b)$$

Now, define a positive function $V = \underline{\omega}^T J \underline{\omega} / 2$. Using the norm inequality²¹ leads to

$$\begin{aligned}\dot{V} &= -2\alpha\gamma V - \alpha\beta\underline{\omega}^T J \underline{q}_{13} \\ &\leq -2\alpha\gamma V + \alpha\beta \|\underline{\omega}\| \|J \underline{q}_{13}\|\end{aligned}\tag{34}$$

For $r_q = 0$, $V \leq e^{-2\alpha\gamma t} V(0)$, which decays to zero for any α . This means that for $r_q = 0$ the controller will always drive the angular velocity to zero. For $r_q \neq 0$, using the well known inequality $ab \leq z a^2 + b^2/(4z)$ for any a, b , and $z > 0$, and defining $z = \alpha\gamma/2\|J^{-1}\|$ yields

$$\dot{V} \leq -2\alpha\gamma V + \frac{\alpha\gamma}{2\|J^{-1}\|} \underline{\omega}^T \underline{\omega} + \frac{\alpha\beta^2}{2\gamma} \|J \underline{q}_{13}\|^2 \|J^{-1}\| \tag{35}$$

Next, use the following inequality

$$\underline{\omega}^T \underline{\omega} \leq \|J^{-1}\| \underline{\omega}^T J \underline{\omega} \tag{36}$$

Also, use the fact that $\|\underline{q}_{13}\|$ is always bounded since $0 \leq q_i \leq 1, i = 1, 2, 3$, so that

$$\|J \underline{q}_{13}\| \leq \|J\| \tag{37}$$

The utilization of these expressions leads to

$$\dot{V} \leq -\alpha\gamma V + \frac{\alpha\beta^2}{2\gamma} \|J\|^2 \|J^{-1}\| \tag{38}$$

Equation (38) cannot be integrated directly because of the time-dependence on the right hand side, but a simple change of the independent variable $\tau = \alpha t$ will eliminate α , leading to

$$V(t) \leq \left[V(0) - \frac{\beta^2}{2\gamma^2} \|J\|^2 \|J^{-1}\| \right] e^{-\alpha\gamma t} + \frac{\beta^2}{2\gamma^2} \|J\|^2 \|J^{-1}\| \tag{39}$$

Since α and γ are always positive, and using Equations (33) and (36), the following equation at steady state is now given

$$\|\underline{\omega}_{ss}\| \leq \frac{2\Delta t r_q}{\Delta t^2 r_q + 8r_\omega} \|J\| \|J^{-1}\| \tag{40}$$

Notice that Equation (40) is no longer a function of $\alpha(t)$, and the angular velocity is always bounded. Also, the factor $f = 2\Delta t r_q (\Delta t^2 r_q + 8r_\omega)^{-1}$ has a maximum at $\Delta t = \sqrt{8r_\omega/r_q}$ sec. If $r_\omega = r_q$ it is easy to see that the factor decreases rapidly below $\Delta t = \sqrt{8}$, and gradually decreases above $\Delta t = \sqrt{8}$ (see Table 1). This is useful for determining a sampling interval which provides robustness in the design.

Table 1 Sampling Interval and Robustness Factor

Δt	f
0.01	0.0025
0.1	0.025
1	0.222
$\sqrt{8}$	0.354
10	0.185
100	0.020

Attitude Tracking

The attitude-only tracking case is easily handled by the predictive controller. For this case the quantities in Equation (21) simply become

$$\Lambda = \frac{\Delta t^2}{2} I_{4 \times 4} \quad (41a)$$

$$\underline{z} = \underline{z}_q \quad (41b)$$

$$S(\underline{x}) = \frac{1}{2} \Xi(\underline{q}) J^{-1} \quad (41c)$$

This is equivalent to setting $r_\omega = 0$ in Equation (29).

A linear analysis for this system can be performed assuming that $W = 0$, and $R = r_q I_{4 \times 4}$.

Euler's equation for this closed-loop case reduces to

$$\dot{\underline{\omega}} = -\frac{2}{\Delta t} \underline{\omega} + \frac{4}{\Delta t^2} \Xi^T(\underline{\tilde{q}}^\Delta) \underline{q} \quad (42)$$

where $\underline{\tilde{q}}^\Delta \equiv \underline{\tilde{q}}(t + \Delta t)$. The linearized kinematic equations for small angle errors are derived in Ref. [22]. Assuming that $\Xi^T(\underline{\tilde{q}}^\Delta) \underline{q} \approx \underline{\delta q}_{13}$ to within first order, the linearized equations of motion can be shown to be given by

$$\dot{\underline{\delta x}} = \begin{bmatrix} -[\underline{\tilde{\omega}} \times] & \frac{1}{2} I_{3 \times 3} \\ -\frac{4}{\Delta t^2} I_{3 \times 3} & -\frac{2}{\Delta t} I_{3 \times 3} \end{bmatrix} \underline{\delta x} \quad (43)$$

with

$$\underline{\delta x} \equiv \begin{bmatrix} \underline{\delta q}_{13} \\ \underline{\omega} - \underline{\tilde{\omega}} \end{bmatrix} \quad (44)$$

The state matrix in Equation (43) can be easily shown to have stable eigenvalues for constant $\underline{\tilde{\omega}}$. This formulation will also be stable for large errors, but experience has shown that it produces large control-input corrections. However, the attitude-only formulation works well when the attitude errors are small, and may be used to ease the computational load.

Attitude Estimation of MAP

In this section, the predictive controller is used to control the attitude of the Microwave Anisotropy Probe (MAP) spacecraft from quaternion observations and gyro measurements. The spacecraft is due to be launched around the year 2000. The main objectives of the MAP mission include: (1) to create a full-sky map of the cosmic microwave background and measure anisotropy with 0.3° angular resolution, and (2) to answer fundamental cosmological questions such as, inflationary versus non-inflationary “big bang” models, accurate determination of the Hubble constant, and the existence and nature of dark matter.

The ideal orbit for the MAP spacecraft is about the Earth-Sun L_2 Lagrange point, which is a Lissajous orbit with approximately a 180-day period. Because of its distance, 1.5 million km from Earth, this orbit affords great protection from the Earth's microwave emission, magnetic fields, and other disturbances, with the dominant disturbance torque being solar radiation pressure. It also provides for a very stable thermal environment and near 100% observing efficiency, since the Sun, Earth, and Moon are always behind the instrument's field of view. In this orbit MAP sees a Sun/Earth angle between 2 and 10 degrees. The instrument scans an annulus in the hemisphere away from the Sun, so the universe is scanned twice as the Earth revolves once around the sun.

The spacecraft orbit and attitude specifications are shown in Figure 1. To provide the scan pattern, the spacecraft spins about the z-axis at 0.464 rpm, and the z-axis cones about the Sun-line at 1 rev/hour. A $22.5^\circ \pm 0.25^\circ$ angle between the z-axis and the Sun direction must be maintained to provide a constant power input, and to provide constant temperatures for alignment stability and science quality. The instrument pointing knowledge is 1.8 arcmin (1σ), which is not required for onboard or real-time implementation.

The attitude determination hardware consists of a Digital Sun Sensor (DSS), Coarse Sun Sensors (CSS's), a star tracker, and gyroscopic rate sensors. The DSS is facing in the plus z (nominal Sun) direction. The star tracker boresight is to be pointed perpendicular to the spin axis, and 22.5° and 157.5° from the instrument apertures. The attitude control hardware includes a Reaction Wheel Assembly (RWA), which consists of three wheels oriented at a common angle

to the spin axis, and distributed equally in azimuth about the spin axis. Also, the wheels torques saturate at 0.1 N-m each.

The spacecraft's attitude is defined by a 3-1-3 Euler angle rotation relative to a rotating, Sun-referenced frame. The three Euler angles are $\tilde{\phi}$, $\tilde{\theta}$, and $\tilde{\psi}$, and the desired states for observing mode are

$$\dot{\tilde{\phi}} = 1 \frac{\text{rev}}{\text{hr}} = 0.001745 \frac{\text{rad}}{\text{sec}} \quad (45\text{a})$$

$$\tilde{\theta} = 22.5^\circ = 0.3927 \text{ rad} \quad (45\text{b})$$

$$\dot{\tilde{\psi}} = 0.464 \text{ rpm} = 0.04859 \frac{\text{rad}}{\text{sec}} \quad (45\text{c})$$

The desired Euler angles for $\tilde{\phi}$ and $\tilde{\psi}$ are determined by integrating the Euler rates. Also, $\dot{\tilde{\theta}}$ is set to zero. The commanded quaternion is determined using

$$\tilde{q}_1 = \sin\left(\frac{\tilde{\theta}}{2}\right) \cos\left(\frac{\tilde{\phi} - \tilde{\psi}}{2}\right) \quad (46\text{a})$$

$$\tilde{q}_2 = \sin\left(\frac{\tilde{\theta}}{2}\right) \sin\left(\frac{\tilde{\phi} - \tilde{\psi}}{2}\right) \quad (46\text{b})$$

$$\tilde{q}_3 = \cos\left(\frac{\tilde{\theta}}{2}\right) \sin\left(\frac{\tilde{\phi} + \tilde{\psi}}{2}\right) \quad (46\text{c})$$

$$\tilde{q}_4 = \cos\left(\frac{\tilde{\theta}}{2}\right) \cos\left(\frac{\tilde{\phi} + \tilde{\psi}}{2}\right) \quad (46\text{d})$$

The kinematic equation that transforms the commanded Euler rates to the commanded body rates is given by

$$\tilde{\omega} = \begin{bmatrix} \sin \tilde{\theta} \sin \tilde{\psi} & \cos \tilde{\psi} & 0 \\ \sin \tilde{\theta} \cos \tilde{\psi} & -\sin \tilde{\psi} & 0 \\ \cos \tilde{\theta} & 0 & 1 \end{bmatrix} \begin{bmatrix} \dot{\tilde{\phi}} \\ \dot{\tilde{\theta}} \\ \dot{\tilde{\psi}} \end{bmatrix} \quad (47)$$

The proposed (on-board) control law is based on a quaternion feedback law derived by Wie and Barba,³ given by

$$\underline{u} = -k_p \underline{\Xi}^T (\tilde{\underline{q}}^{-1}) \underline{q} - k_d (\underline{\omega} - \tilde{\underline{\omega}}) = -k_p \underline{\delta q}_{13} - k_d (\underline{\omega} - \tilde{\underline{\omega}}) \quad (48)$$

Also, the problem of re-orientating a rigid spacecraft with control constraints has been executed using cascade-saturation control logic (see Ref. [23] for details). Linearized equations of motion can also be derived using the quaternion feedback (QF) control scheme shown in Ref. [3], given by

$$\underline{\delta \dot{x}} = \begin{bmatrix} -[\tilde{\underline{\omega}} \times] & \frac{1}{2} I_{3 \times 3} \\ -k_p J^{-1} & A_{22} \end{bmatrix} \underline{\delta x} \quad (49)$$

where

$$A_{22} = J^{-1} \{ -[\tilde{\underline{\omega}} \times] J + [J \tilde{\underline{\omega}} \times] \} - k_d J^{-1} \quad (50)$$

It can be easily shown that this system is unstable if $k_d = 0$. Therefore, attitude-only tracking cannot be implemented using this scheme.

A number of simulation studies have been performed comparing the quaternion feedback scheme with the predictive controller. The initial conditions for the simulations are set to zero for both the attitude and rate terms. For the predictive filter two cases are used. The first one uses the basic control law shown in Equation (21) with a saturator applied to the right hand side for enforcement of the control bounds (i.e., a non-optimal solution). The second case solves the constrained predictive control problem using the iterative technique given by Equation (24). The two cases are in fact equivalent if the assumed inertia matrix is diagonal. However, significant differences arise even for small off-diagonal quantities. This is shown in Figure 2, where the angle of axis rotation error corresponds to the angle θ in Equation (2) using the error quaternion. Clearly, using the iterative scheme produces better performance. This is also shown for the control input comparison in Figure 3. The iterative control scheme requires less switches and control effort than constraining the control output directly.

The next simulation study involves a comparison between the optimal predictive filter and an optimal quaternion feedback scheme. Gains for the quaternion feedback controller were found by minimizing a quadratic cost function, similar to a linear-quadratic cost function. Also, 5% errors were introduced in the assumed inertia matrix. A comparison plot of the quaternion feedback and predictive controller eigenaxis-rotation angle error is shown in Figure 4. Clearly, the predictive filter outperforms the quaternion feedback controller. Also, the steady-state errors are reduced significantly with the predictive filter. The quaternion feedback case produces a steady-state pitch error of approximately 0.01° . This error can only be reduced slightly by using integral control. It can be further reduced by using a feedforward acceleration term. This essentially determines an added torque to reduce the steady-state error. However, this method can be sensitive to modeling errors in the inertia matrix. The predictive controller produced a steady-state error that is significantly lower ($\theta_{ss} \approx 1 \times 10^{-4}$ deg) than the quaternion feedback controller. Also, the predictive controller requires less torque to achieve this performance, as seen in Figure 5. A plot of the predictive controller phase error portrait is shown in Figure 6. Finally, a plot of the predictive filter with quaternion-tracking for a relatively small initial error is shown in Figure 7. This clearly shows that a quaternion-tracking predictive controller can stabilize a spacecraft.

The next simulation case shows comparative results for disturbance rejection. The dominant source of disturbance for MAP is solar radiation pressure torque. The instantaneous magnitude of this torque is approximately 1×10^{-5} N-m. The spacecraft symmetry and spin will decrease the long-term average. For simulation purposes a magnitude 10 times greater than the approximate value is used. The geometric figure of the spacecraft is assumed to be a plane. Force and torque equations for this simple geometric figure are shown in Ref. [24]. A plot of the tracking errors with a solar pressure disturbance is shown in Figure 8. Clearly, the predictive controller is able to reject disturbance torques more effectively than the quaternion feedback controller.

Conclusions

In this paper, a new approach for the control of a spacecraft with large angle maneuvers was presented. The new approach was developed using a model-based strategy to predict control

torques, so that a continuous minimization of the tracking errors is achieved. Formulations were presented which use either attitude and rate tracking or attitude tracking solely. Also, the robustness of the new controller for errors in the assumed inertia matrix was shown. Next, a simulation study was shown comparing the new controller with a more traditional proportional-derivative type controller for the Microwave Anisotropy Probe spacecraft. Results indicate that the predictive controller converges to the desired values faster than the traditional controller, and provides nearly unbiased tracking errors.

Acknowledgments

The first author's work was partially supported by a National Research Council Postdoctoral Fellowship tenured at NASA-Goddard Space Flight Center. The author greatly appreciates this support. Also, the author wishes to thank Dr. Ping Lu of Iowa State University and Dr. Panagiotis Tsotras of the University of Virginia for many interesting and helpful discussions.

References

- ¹Scrivener, S.L., and Thompson, R.C., "Survey of Time-Optimal Attitude Maneuvers," *Journal of Guidance, Control and Dynamics*, Vol. 17, No. 2, March-April 1994, pp. 225-233.
- ²Vadali, S.R., and Junkins, J.L., "Optimal Open-Loop and Stable Feedback Control of Rigid Spacecraft Maneuvers," *The Journal of the Astronautical Sciences*, Vol. 32, No. 2, April-June 1984, pp. 105-122.
- ³Wie, B., and Barba, P.M., "Quaternion Feedback for Spacecraft Large Angle Maneuvers," *Journal of Guidance*, Vol. 8, No. 3, May-June 1985, pp. 360-365.
- ⁴Tsotras, P., "Stabilization and Optimality Results for the Attitude Control Problem," *Journal of Guidance, Control and Dynamics*, Vol. 19, No. 4, July-Aug, 1996, pp. 772-779.
- ⁵Shuster, M.D., "A Survey of Attitude Representations," *The Journal of the Astronautical Sciences*, Vol. 41, No. 4, Oct.-Dec. 1993, pp. 439-517.
- ⁶Slotine, J.J.E., and Li, W., *Applied Nonlinear Control*, Prentice Hall, NJ, 1991.

⁷Ramirez, H.S., and Dwyer, T.A.W., "Variable Structure Control of Spacecraft Reorientation Maneuvers," *Proceedings of AIAA Guidance, Navigation, and Control Conference*, Williamsburg, VA, Aug. 1986, AIAA Paper #86-1987, pp. 88-96.

⁸Vadali, S.R., "Variable Structure Control of Spacecraft Large Angle Maneuvers," *Journal of Guidance, Control and Dynamics*, Vol. 9, No. 2, March-April 1986, pp. 235-239.

⁹Crassidis, J.L., and Markley, F.L., "Sliding Mode Control Using Modified Rodrigues Parameters," *Journal of Guidance, Control and Dynamics*, Vol. 19, No. 6, Nov.-Dec. 1996, pp. 1381-1383.

¹⁰Kang, W., "Nonlinear H_∞ Control and Its Application to Rigid Spacecraft," *IEEE Transactions on Automatic Control*, Vol. 40, No. 7, July 1995, pp. 1281-1285.

¹¹Schaub, H., Junkins, J.L., and Robinett, R.D., "Adaptive External Torque Estimation By Means of Tracking a Lyapunov Function," *AAS/AIAA Space Flight Mechanics Meeting*, Austin, TX, Feb. 1996, AAS Paper #96-172.

¹²Chu, D., and Harvie, E., "Accuracy of the ERBS Definitive Attitude Determination System in the Presence of Propagation Noise," *Proceedings of the Flight Mechanics/Estimation Theory Symposium*, NASA-Goddard Space Flight Center, Greenbelt, MD, 1990, pp. 97-114.

¹³Challa, M.S., Natanson, G.A., Baker, D.E., and Deutschmann, J.K., "Advantages of Estimating Rate Corrections During Dynamic Propagation of Spacecraft Rates-Applications to Real-Time Attitude Determination of SAMPEX," *Proceedings of the Flight Mechanics/Estimation Theory Symposium*, NASA-Goddard Space Flight Center, Greenbelt, MD, 1994, pp. 481-495.

¹⁴Crassidis, J.L., and Markley, F.L., "Predictive Filtering for Attitude Estimation Without Rate Sensors," *Journal of Guidance, Control and Dynamics*, Vol. 20, No. 3, May-June 1997, pp. 522-527.

¹⁵Lizarralde, F., and Wen, J.T., "Attitude Control Without Angular Velocity Measurement: A Passivity Approach," *IEEE Transactions on Automatic Control*, Vol. 41, No. 3, March 1996, pp. 468-472.

¹⁶Lu, P., "Nonlinear Predictive Controllers for Continuous Systems," *Journal of Guidance, Control and Dynamics*, Vol. 17, No. 3, May-June 1994, pp. 553-560.

¹⁷Lu, P., "Constrained Tracking Control of Nonlinear Systems," *System and Control Letters*, Vol. 27, 1996, pp. 305-314.

¹⁸Khan, M.A., and Lu, P., "New Technique for Nonlinear Control of Aircraft," *Journal of Guidance, Control and Dynamics*, Vol. 17, No. 5, Sept.-Oct. 1994, pp. 1055-1060.

¹⁹Markley, F.L., "Equations of Motion," *Spacecraft Attitude Determination and Control*, Wertz, J.R., (editor), Kluwer Academic Publishers, Dordrecht, 1978, pp. 521-523.

²⁰Shuster, M.D., "The Quaternion in the Kalman Filter," *AAS/AIAA Astrodynamics Specialist Conference*, Victoria, BC, Canada, Aug. 1993, AAS Paper #93-553.

²¹Horn, R.A., and Johnson, C.R., *Matrix Analysis*, Cambridge University Press, Cambridge, MA, 1991.

²²Lefferts, E.J., Markley, F.L., and Shuster, M.D., "Kalman Filtering for Spacecraft Attitude Estimation," *Journal of Guidance, Control and Dynamics*, Vol. 5, No. 5, Sept.-Oct. 1982, pp. 417-429.

²³Wie, B., and Jiambo, L., "Feedback Control Logic for Spacecraft Eigenaxis Rotations Under Slew Rate and Control Constraints," *Proceedings of AIAA Guidance, Navigation, and Control Conference*, Scottsdale, AZ, Aug. 1994, AIAA Paper #94-3563, pp. 197-206.

²⁴Spence, J.B., "Environmental Torques," *Spacecraft Attitude Determination and Control*, Wertz, J.R., (editor), Kluwer Academic Publishers, Dordrecht, 1978, pp. 570-573.

Fig. 1 MAP Spacecraft Specifications

Fig. 2 Optimal and Non-Optimal Predictive Control

Fig. 3 Optimal and Non-Optimal Predictive Control

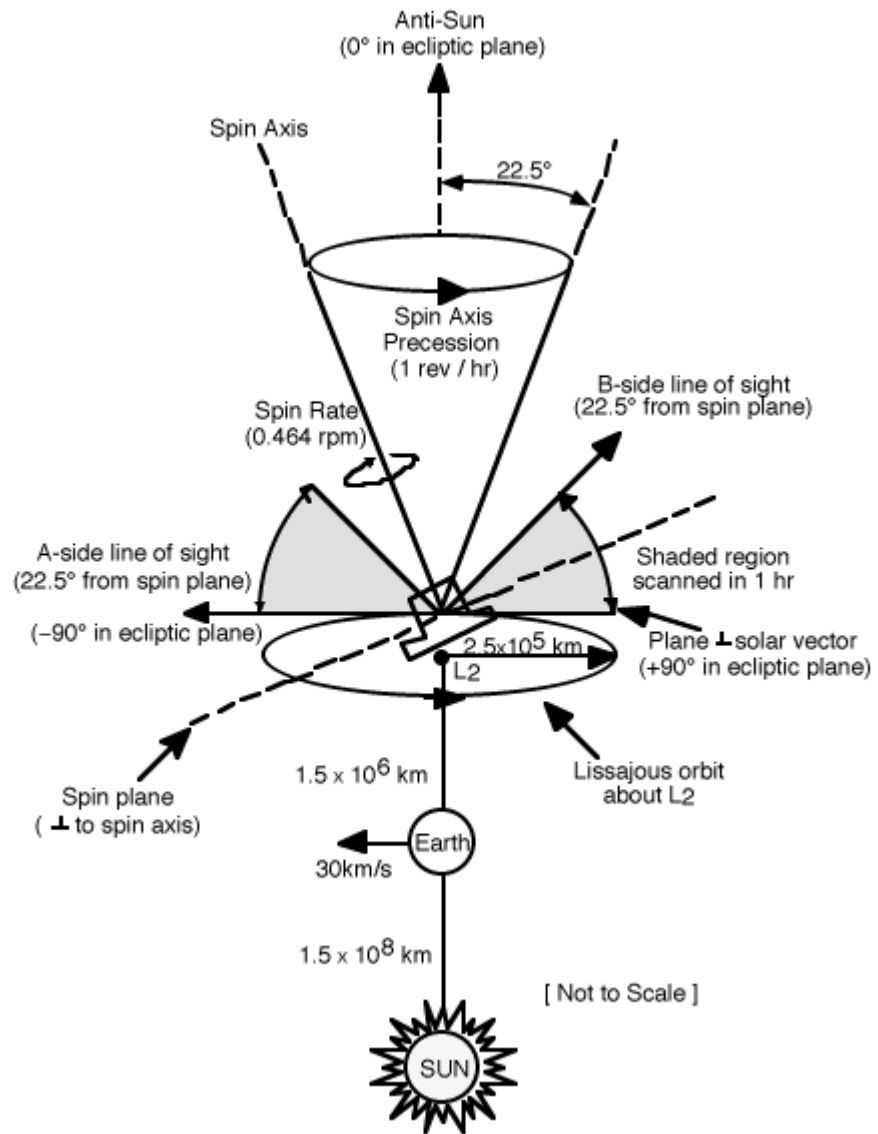
Fig. 4 Quaternion and Optimal Predictive Control

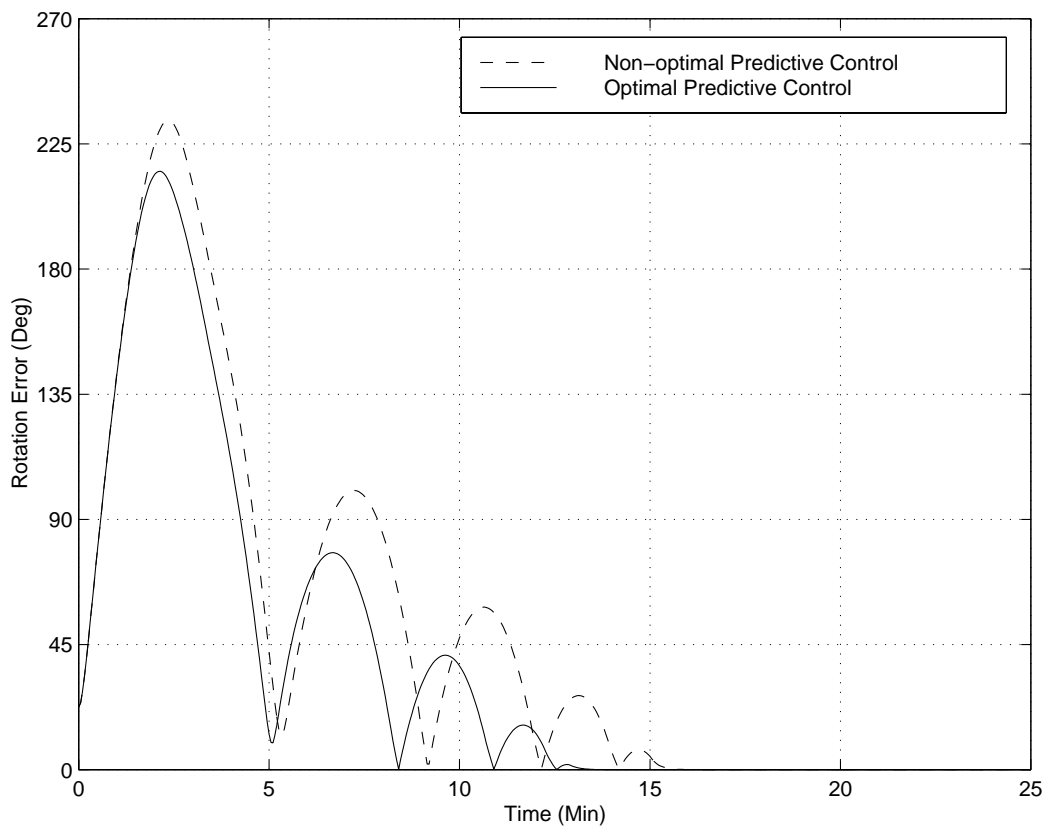
Fig. 5 Quaternion and Optimal Predictive Control

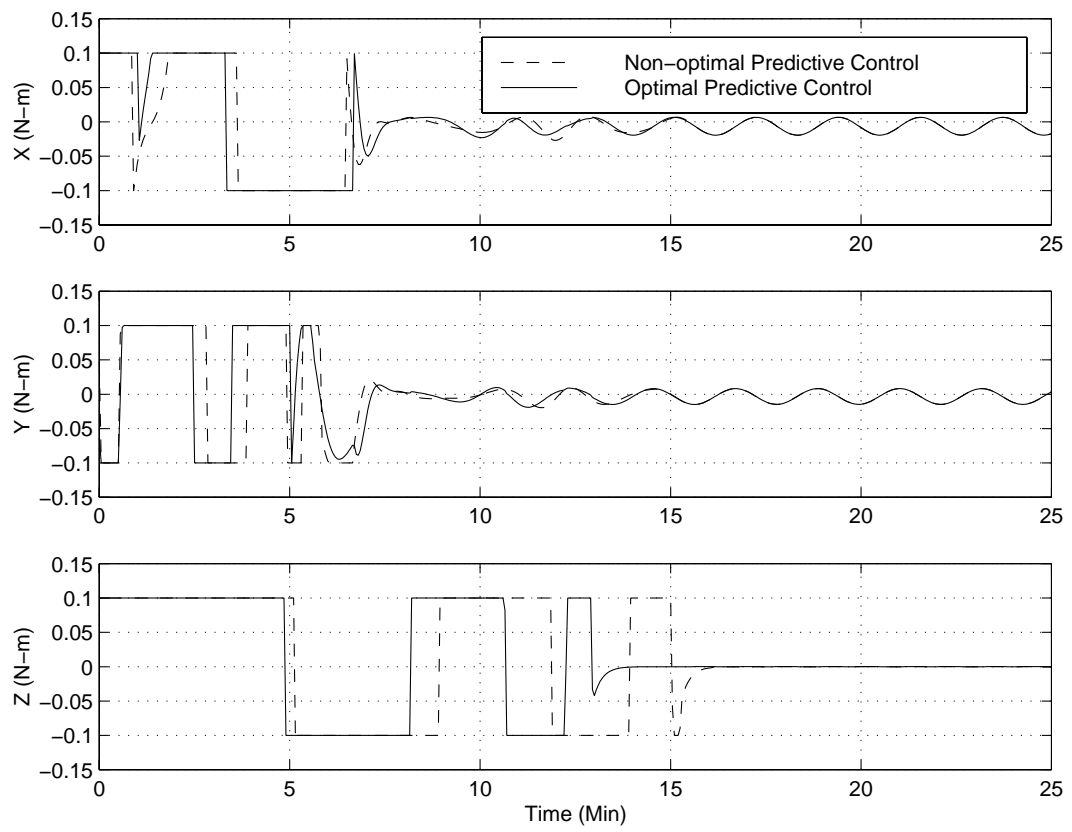
Fig. 6 Phase Portrait Plot

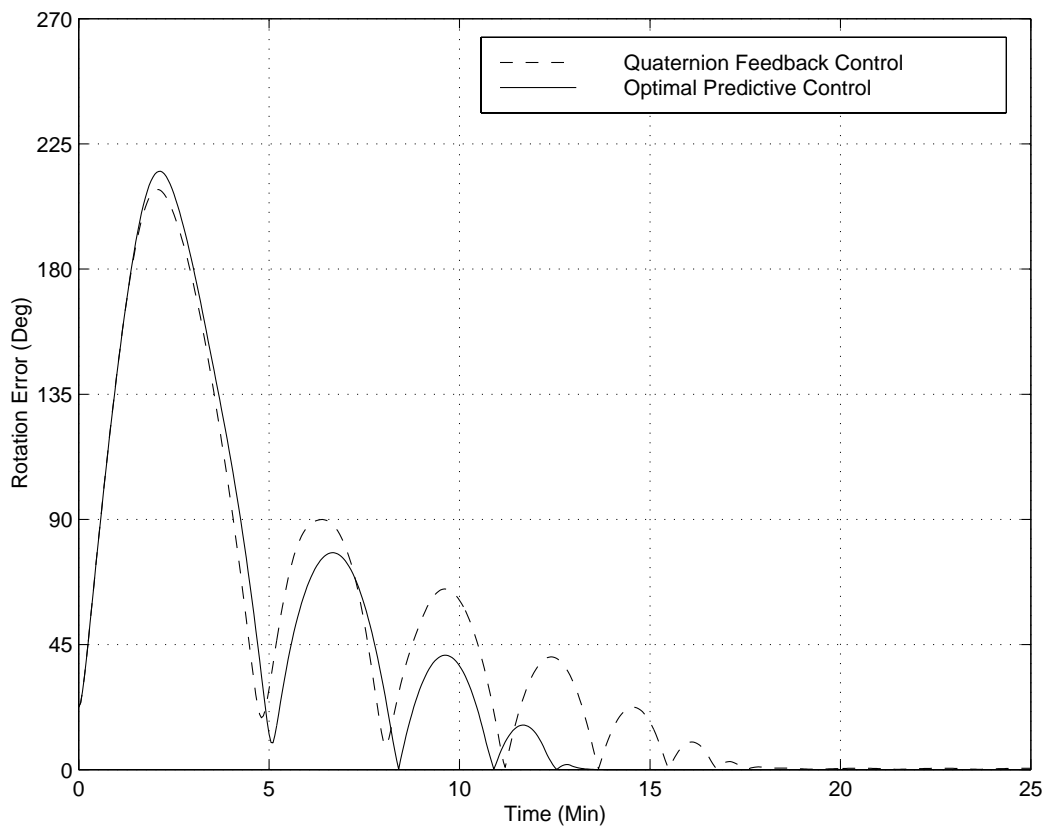
Fig. 7 Quaternion-Tracking Predictive Control

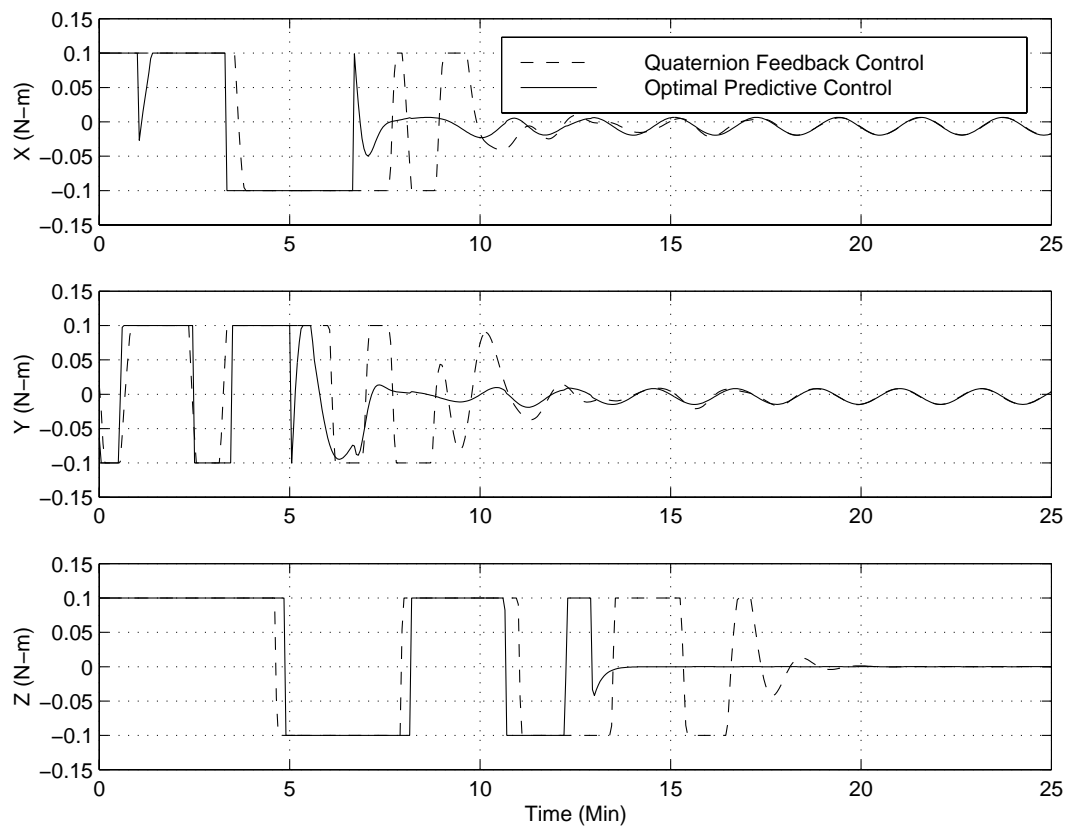
Fig. 8 Disturbance Rejection Comparison











Angle Error Plot for Optimal Predictive Controller

